

Ekman layers and two-dimensional frontogenesis in the upper ocean

LuAnne Thompson

School of Oceanography, University of Washington, Seattle

Abstract. A two-dimensional modified semi geostrophic model is used to study the evolution of oceanic fronts in the presence of vertical mixing. The parameterization used for mixing is an elevated constant value of vertical viscosity and friction; hence the Ekman layer acts as a surrogate mixed layer, with, however, vertical shear allowed everywhere. An initial condition representative of the observed fields in Frontal Air-Sea Interaction Experiment (FASINEX) is used, and its modification in the presence of vertical mixing alone is investigated. Without external forcing an Ekman layer results because of the presence of vertical geostrophic shear at the surface. The maximum density gradient moves toward the dense side of the front driven by this flow. Convergence of Ekman flow results in downward bowing of the isopycnals beneath the surface expression of the front, a feature reminiscent of density sections taken during FASINEX. This feature is not evident when a barotropic convergence field is applied in the absence of mixing or in fully nonlinear simulations of the evolution of fronts with baroclinic instability. An analytic theory suggests that the maximum density gradient will increase over time when vertical mixing alone is present. In the presence of negative uniform wind stress in the direction opposite to the surface geostrophic flow the front moves toward the denser water, and the jet uniformly decreases in strength. In the presence of a positive uniform wind in the direction of the surface geostrophic flow the surface jet initially weakens but then strengthens again as the wind-driven Ekman flow opposes the frictionally driven Ekman flow and the cross-front density gradient increases.

1. Introduction

Fronts manifest themselves in the ocean in several different ways. Both property fronts with little dynamical signature and density fronts with associated near-surface geostrophic shear occur throughout the ocean interior. Examples of zones in the ocean where density fronts occur are regions of large-scale Ekman convergence, such as the subtropical front in the North Atlantic [Eriksen *et al.*, 1991; Pollard and Regier, 1992] and the North Pacific [Roden, 1980]. Density fronts with cross-frontal scales of order 10 km often occur within these zones. These smaller-scale frontal features are distinct from the large-scale changes in thermocline depth that make up the wind-driven general circulation. The small-scale fronts have been associated with localized large vertical velocities and enhanced mixing. Near these density fronts are larger-scale mesoscale features [Voorhis *et al.*, 1976] that apparently force them. The mesoscale features may be formed by larger-scale baroclinic instability of the thermocline. The small-scale fronts themselves also may be baroclinically unstable, which can lead in turn to smaller frontal features within the evolving baroclinic field.

Dynamical understanding of oceanic fronts has come in large part from the atmospheric sciences, where models of fronts were first developed. These models were designed to provide understanding of frontogenesis driven by baroclinic instability. The classic inviscid frontal model of Hoskins and Bretherton [1972] (hereinafter referred to as HB) uses the most

unstable Eady mode as forcing to create a two-dimensional model of frontogenesis. Using the semigeostrophic approximation (in which the along-front length scale is assumed to be much larger than the cross-front length scale), HB showed that a barotropic external deformation field applied to a uniform horizontal density gradient causes a finite discontinuity in density to develop at the surface in finite time. This result is in contrast to a purely quasi-geostrophic model in which the surface discontinuity forms as time goes to infinity. Mixing or friction and three-dimensional effects would eventually take over to smooth out discontinuities. In the ocean the mixed layer is most likely of importance to the dynamics of fronts. A distinguishing characteristic of oceanic density fronts that contrasts with atmospheric fronts is that the vertical penetration scale of the mixed layer can often be a significant fraction of the vertical scale of the front itself and thus cannot necessarily be separated from the bulk structure of the density front.

Modeling of open ocean fronts has progressed along two lines. First, the two-dimensional (cross-frontal and vertical) approach following HB has been used by several authors to study frontogenesis by a barotropic convergence field and by wind-driven convergence. MacVean and Woods [1980] applied the inviscid ideas of HB to a density field representative of that in the ocean. In particular, they include an unstratified layer on top of a stratified layer to represent the mixed layer. They find that low Richardson numbers appear near the front as it sharpens. Also, mixed layer water appears to be pulled down in the water column, suggesting that it could be subducted. This model allows vertical shear to develop throughout the upper ocean. A similar study is that done by Bleck *et al.* [1988], who used a two-dimensional isopycnal model to study the same

Copyright 2000 by the American Geophysical Union.

Paper number 1999JC900336.
0148-0227/00/1999JC900336\$09.00

process. In contrast, models have also been developed including a mixed layer that can entrain deep ocean water [Rudnick and Davis, 1988; Cushman-Roisin, 1981] to allow mixing processes that are present in the mixed layer. Adamec and Garwood [1985] explore the response of the Maltese front to wind and buoyancy forcing in a two-dimensional primitive equation model that was coupled to a one-dimensional mixed layer. In studies in which a traditional mixed layer is included, both the density and the velocity are assumed to remain vertically uniform within the mixed layer through continuous mixing despite large horizontal density gradients (and potential generation of near-surface geostrophic shear). Nonhydrostatic simulations show evidence of modification of fronts by wind [Lee et al., 1994], while in nonhydrostatic and primitive equation simulations, inertial oscillations tend to dominate the calculations.

The second modeling approach used in the study of oceanic fronts is the investigation of the evolving three-dimensional structure owing to baroclinic instability. Both the linear and nonlinear evolutions via baroclinic instability have been studied [e.g., Samelson, 1993; Samelson and Chapman, 1995; Spall, 1995; Boss et al., 1996]. With the nonlinear studies it is clear that the front can sharpen in crests of the baroclinic waves. These studies have concentrated on density fronts such as those observed in Frontal Air-Sea Interaction Experiment (FASINEX) [Eriksen et al., 1991; Pollard and Regier, 1992], and it has been shown that initially the evolution can be predicted well from quasi-geostrophic theory [Samelson, 1993; Boss et al., 1996], suggesting that the approach of HB of using a simple representation of a quasi-geostrophic Eady mode to force frontogenesis is reasonable. The maximum downwelling velocity in a fully nonlinear simulation is $\sim 37 \text{ m d}^{-1}$ after 3 days [Samelson and Chapman, 1995]. Presumably, this vertical velocity could move fluid parcels from the surface to depth. However, in the models used to study the three-dimensional structure of fronts, diapycnal mixing has been reduced as much as possible, and an active mixed layer is missing. For permanent transfer of parcels from the surface to depth or across the front horizontally, there must be some nonconservative process to allow fluid parcels to cross density surfaces. Spall [1997] studied whether an unstable front could equilibrate in the presence of an external convergence field. Under certain parameter regimes he found that when the deformation field is strong enough, the front can equilibrate, and at that point, subgrid-scale mixing processes become important. In general, the ageostrophic cross-front circulation and heat flux are dominated by that resulting from the convergence field. The dynamics of the equilibrated front are fundamentally two-dimensional.

In order to analyze whether theoretical ideas can be applied to observed oceanic fronts, Pollard and Regier [1992] explored the FASINEX front by making a series of density and velocity sections using acoustic Doppler current profile (ADCP) and SeaSoar instruments. Nine density sections were made, and in each section a thick mixed layer appears on the dense side of the front. One of these density sections provides the initial conditions for the work of Samelson [1993] and Samelson and Chapman [1995]. As the layer defined by isopycnals that outcrop there descends, visual inspection shows that in six of the nine sections the layer is relatively thick below the maximum horizontal density gradient at the surface. Pollard and Regier [1992] argue that this gives evidence of advection of the mixed layer water downward. We will argue here that this feature depends on frictionally driven convergence. They also derive

the cross-front vertical flow by making simplifying assumptions (i.e., there is no along-front variability, and the flow is inviscid and purely geostrophic) and applying ideas first introduced by HB. Results of this diagnostic calculation will be discussed in the context of our model results. Rudnick [1996] does a similar three-dimensional inversion for the vertical velocity field and finds that there is a tendency for denser water to be downwelled and warmer water to be upwelled, in the typical thermally direct sense, and finds a maximum vertical velocity field of $\sim 17 \text{ m d}^{-1}$. This calculation was done using the quasi-geostrophic omega equations, as was that done by Pollard and Regier [1992]. Rudnick [1996] also finds that the changes in the density field come about mostly through horizontal advection, which we will show is consistent with the ideas presented in this paper.

To investigate the influence of mixing on small-scale fronts, we use a model that has high vertical mixing and at the same time allows vertical density gradients and vertical shear near the surface. We do not consider the full three-dimensional influence of baroclinic instability but, instead, use a two-dimensional (cross-front and vertical) continuously stratified finite difference model to study the evolving front. The influence of baroclinic instability is modeled qualitatively by the inclusion of a barotropic convergence field as by HB. We also follow HB and apply the semigeostrophic approximation so that ageostrophic effects that are crucial to the frontogenesis process can be studied while removing the confounding effects of gravity waves. The mixing is parameterized as vertical Laplacian friction and represents the turbulence owing to surface processes (gravity waves, wind, etc.) that are the primary causes of vertical transport of momentum and density in the upper ocean. This parameterization is consistent with the idea that mixing processes in the upper ocean are well represented by one-dimensional mixed layer models. However, with explicit vertical mixing, but not complete homogenization as is assumed in mixed layer models, isopycnals and other property contours can slope in the surface layer. This addition allows us to apply the theory of Ekman layers and study the influence of the associated vertical shear on the detailed evolution of the front in a simple model.

This work follows that of Garrett and Loder [1981]. In that study a simple formula was derived for the cross-frontal flow induced by friction, parameterized in terms of an eddy viscosity coefficient under the approximation that the Rossby number and Ekman number are small. The equation applies to the region outside of the surface Ekman layer, where isopycnal depths satisfy a diffusion equation with a diffusion coefficient that depends on the local buoyancy frequency. If density diffusion is added, Garrett and Loder [1981] showed that there is an additional term that acts to sharpen gradients in isopycnal depth in the cross-isopycnal direction. Several predictions were made from this study, including that near the surface, there will be a sharpening of the horizontal density gradient on the denser side of the front. Many of the results found in the work presented here were suggested by their analytic work.

The outline of the paper is as follows. A description of the model is given followed by an application using the barotropic convergence field of HB and no vertical mixing. Next, the spindown of the same density front is described, and the combined effect of mixing and barotropic convergence is presented. Finally, the influence of the wind on the evolution of the front is explicated, and consequences of the modeling results are discussed. In the appendix a semianalytic solution is

found for the surface density distribution under simplifying assumptions, and comparisons are made to the numerical model results.

2. Model Formulation

A modified semigeostrophic model is presented that we use to identify how Ekman layers in the ocean interfere with or contribute to frontogenesis. Vertical mixing is added to the semigeostrophic model described above. This approach provides a qualitative look at the highly mixed upper ocean, while allowing vertical shear and vertical density gradients near the surface. The value of the vertical mixing parameter in this study is enhanced over a typical value of diapycnal (or vertical) mixing in the ocean interior so that the Ekman layer acts as a surrogate mixed layer. The value used in the examples shown below is $0.05 \text{ m}^2 \text{ s}^{-1}$, giving an Ekman layer thickness ($\sqrt{2\nu/f}$) of 32 m. We are assuming that even in the absence of a mean wind, there may be wind events that would cause mixing when the average wind (say, over an inertial period) is zero. Although the actual choice of the size of the frictional coefficient is important, since its primary influence is through the generation of Ekman layers and their convergence, the qualitative results of this study should still hold with other choices (below we show the results with two other values). A further justification for this value comes from the work of *Lee and Eriksen* [1996], who find an equivalent value for the FASINEX region of $0.03 \text{ m}^2 \text{ s}^{-1}$ and a typical wind stress value of 0.1 Pa. It is somewhat artificial to consider friction separate from wind-induced mixing, but it will allow us to examine the frictionally driven and wind-driven Ekman layers separately. At small-scale fronts in the upper ocean, there is more motivation for vertical mixing than horizontal mixing since much of the energy for mixing comes from the surface. Horizontal mixing would also affect the front but is not discussed in detail here.

With vertical mixing included the formulation of the modified semigeostrophic two-dimensional model is as follows: the cross-front momentum balance is between the Coriolis force, the pressure gradient, and vertical mixing (with vertical friction ν),

$$-fv = -P_x + \nu u_{zz}. \quad (1)$$

The along-front velocity can then be divided into a geostrophic part and an ageostrophic part that is driven by friction,

$$v = v_g + v_a. \quad (2)$$

The geostrophic part is by definition balanced exactly by the cross-front pressure gradient, $fv_g = P_x$, while the ageostrophic part is balanced by mixing of cross-front momentum, $fv_a = -\nu u_{zz}$. Thermal wind still applies to the geostrophic velocity,

$$fv_{gz} = -\frac{g}{\rho_0} \rho_x. \quad (3)$$

The along-front momentum balance is then

$$\frac{Dv_g}{Dt} + fv = -P_y + \nu(v_a + v_g)_{zz}, \quad (4)$$

so only the geostrophic along-front velocity is advected by the total velocity field. The cross-front velocity is purely ageostrophic. The two-dimensional model still strictly applies as long as there are no changes in the along-front direction, but advection of the ageostrophic part of the along-front flow is neglected. This is consistent with the usual application of the geostrophic

momentum approximation [*Hoskins*, 1975] and allows the examination of the influence of friction in a nonlinear and non-quasi-geostrophic setting. Density is also mixed in the vertical, so

$$\frac{D\rho}{Dt} = \kappa\rho_{zz}. \quad (5)$$

This set of equations (1)–(5) is similar to that studied by *Garrett and Loder* [1981]. By choosing a small Rossby number and Ekman number, they ignored the mixing term in the cross-front momentum balance, which we retain here. This retention allows a consistent mass balance near the surface and a full representation of the Ekman layer. *Garrett and Loder* [1981] only considered the vertically integrated effects of the Ekman layer. Here we are interested in the details of the advective effects of the secondary circulation. Their importance is demonstrated, particularly in the vicinity of the front. This system of equations conserves potential vorticity in the absence of vertical mixing where

$$q = \rho_x v_z - \rho_z (v_x + f). \quad (6)$$

The potential vorticity is composed of both tilting vorticity and stretching vorticity.

Because of the presence of vertical mixing, the system of equations can no longer be solved in a Lagrangian (geostrophic coordinates) framework. Instead, an elliptic equation for the cross-front stream function ψ is used. To derive the equation, we take the x derivative of (5) and subtract it from the z derivative of (4). Then, the thermal wind balance (3) is used to eliminate the time derivatives. The resulting equation is linear in ψ and is given by

$$(f + v_x)\psi_{zz} - 2v_{gz}\psi_{xz} - \frac{g}{\rho_0 f} \rho_z \psi_{xx} = -\nu v_{zzz} + \frac{g}{\rho_0 f} \kappa \rho_{zzz}, \quad (7)$$

where $u = \psi_z$ and $w = -\psi_x$. The ageostrophic along-front velocity can be related to the stream function,

$$-fv_a = \nu u_{zz} = \psi_{zzz}, \quad (8)$$

so the right-hand side of (7) can be written $= -(\nu^2/f)\psi_{zzzzz}$ for a Prandtl number (ν/κ) of 1. The Prandtl number could take any value, but a value of 1 is consistent with the mixing schemes of one-dimensional mixed layer models and will be assumed henceforth.

HB applied a barotropic convergent field, geostrophically balanced, so that the velocities and pressure are given by

$$u = -\alpha x + u'(x, z, t), \quad (9)$$

$$v = \alpha y + v'(x, z, t), \quad (10)$$

$$p = f\alpha xy - \alpha^2 y^2/2 + p'(x, z, t). \quad (11)$$

This application results in the same set of equations (1)–(5) for the primed quantities, with the advection modified to

$$\frac{D\phi}{Dt} = \frac{\partial\phi}{\partial t} + (u - \alpha x) \frac{\partial\phi}{\partial x} + w \frac{\partial\phi}{\partial z}, \quad (12)$$

where the primes have now been dropped.

All of the y dependence drops out. To incorporate a barotropic convergence field into the model, (12) is used for the convective derivative, and there is an additional source term in (7) composed of

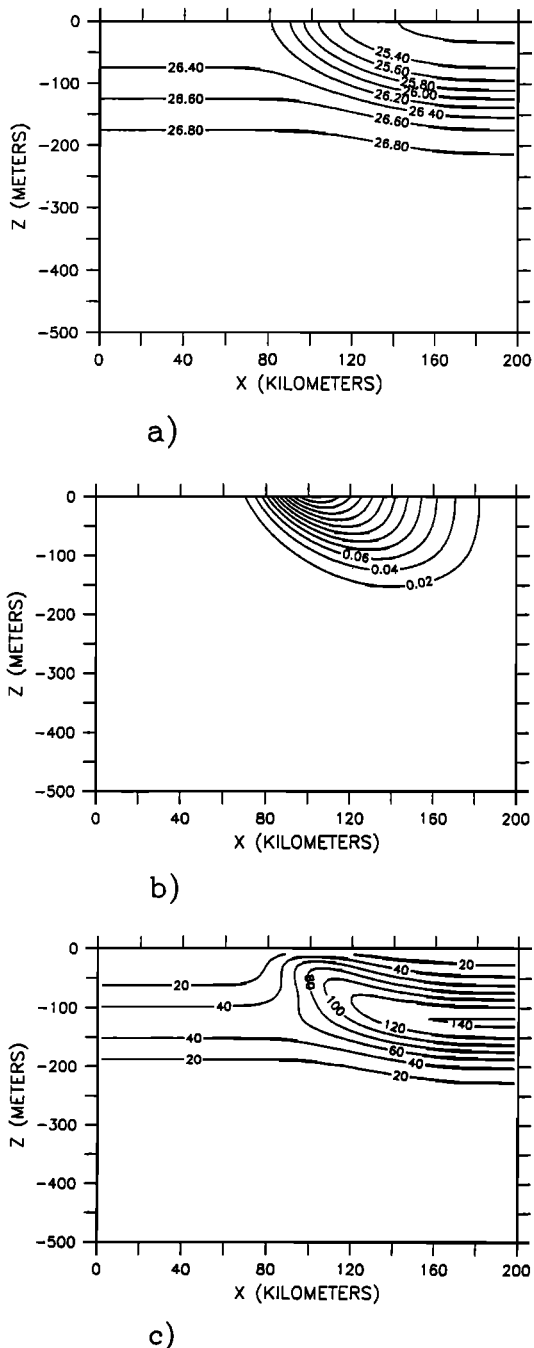


Figure 1. Initial conditions for model runs given by (24): (a) cross-front density ($\text{kg m}^{-3} - 1000$), (b) along-front geostrophic velocity (m s^{-1}), and (c) potential vorticity time $1 \times 10^8 \text{ kg m}^{-4} \text{ s}^{-1}$.

$$\alpha \frac{g\rho_x}{f\rho_0}. \quad (13)$$

The cross-front stream function is solved in a finite difference framework, with a direct procedure for finding the ageostrophic stream function. We use the Arakawa Jacobian (which takes advantage of the velocity being written as a stream function) for the advection of the density and an implicit time-stepping scheme for the frictional part of the density equation. The static stability requirement is occasionally violated. We have included a convective adjustment scheme to take care of

this. Convective adjustment occurs by checking for unstable regions in the water column. If they are found, a simple average of the densities in the vertical down to the point of instability until the water column is stabilized is performed. More sophisticated mixing routines could be incorporated; however, we expect that the qualitative results of this study are independent of the convective adjustment scheme.

The model is run in a fixed box of uniform depth. There is no flow through the top ($z = H$) and bottom ($z = 0$) of the box,

$$\psi = 0 \quad z = 0, H. \quad (14)$$

This assumption requires that the vertical velocity goes to zero at the bottom of the box. There is no across-front stress on the top and bottom of the box,

$$u_z = 0 \quad z = 0, H. \quad (15)$$

We assume that there is no stress along the front on the bottom of the box,

$$(v_g + v_a)_z = 0 \quad z = 0. \quad (16)$$

The total stress at the top of the box is given by the wind,

$$v(v_g + v_a)_z = \frac{\tau^y}{\rho_0} \text{ at } z = H, \quad (17)$$

where τ^y is the wind-stress along the front. Assuming that the vertical side walls are far enough away from regions of strong density gradient, there is no horizontal velocity at the sides of the box in the absence of wind-stress,

$$\psi = 0 \quad x = \pm L. \quad (18)$$

In addition, there is no flux of density through the sides of the box,

$$\rho_x = 0 \quad x = \pm L. \quad (19)$$

The density at the bottom of the box is given by the deep ocean value,

$$\rho = \rho_b \quad z = 0. \quad (20)$$

Finally, there is no flux of density through the top of the box (i.e., there is no heating or cooling or fresh water flux there),

$$\rho_z = 0 \quad z = H. \quad (21)$$

Away from regions of vertical and horizontal shear, and therefore horizontal density gradients (so $v_g = 0$), the frictional part of the along-front flow obeys an Ekman balance,

$$-fv_a = \nu u_{zz}, \quad (22)$$

$$fu = \nu v_{zz}. \quad (23)$$

This fact is used to construct the open boundary conditions at $x = \pm L$ when there is a wind stress applied. The model domain is 500 m in the vertical by 200 km in the horizontal unless otherwise noted. The maximum vertical velocity is located near the surface, well away from the bottom of the box. This suggests that changing the size of the box would not significantly change the results.

3. Model Results: Application to the FASINEX Front

As an initial condition, we employ a similar profile to that used by *Samelson* [1993] in his linear stability calculations of

Table 1. Parameters for Initial Density Field

Parameter	Value
b_f	$-0.6g/\rho_0$
b_b	$b_f/2$
z_0	0.75
x_0	1.0
α	-1.185
d_0	0.125
d_1	0.125
γ	0.05

the FASINEX front, modified to allow the domain size to be larger and with a smaller initial geostrophic velocity (Figure 1a). An analytical representation is used where the initial buoyancy profile $b = g\rho/\rho_0$ in m s^{-2} is given by

$$b = \frac{1}{2}b_f \tanh \{[z - \alpha(x - x_0)^3 - z_0]/d_0\} + \frac{1}{2}b_b \tanh [(z - z_0)/d_1] - \frac{a}{\gamma} \exp [(z - 1)/\gamma], \quad (24)$$

where

$$a = \frac{b_f}{d_0} \text{sech}^2 \{[1 - \alpha(x - x_0)^3 - z_0]/d_0\} + \frac{b_b}{d_1} \text{sech}^2 [(1 - z_0)/d_1]. \quad (25)$$

This function is constructed such that away from the front, the geostrophic velocity goes to zero. The above expression is in nondimensional units such that x and z both span from 0 to 1. The parameters in the above expression are given in Table 1. Another initial condition is also used below following *MacVean and Woods* [1980].

The maximum geostrophic velocity in this configuration 0.22 m s^{-1} (Figure 1b). The initial condition used here has a weaker maximum velocity than the one used by *Samelson* [1993] for his stability calculation, although the form of the front is the same. This weaker front allows us to trace its evolution for a longer period of time, up to the point where baroclinic instability would begin to break the two-dimensional nature of the front. Both the linear stability and the nonlinear evolution of this density section have been explored [*Samelson*, 1993; *Samelson and Chapman*, 1995] where qualitative agreement is found with certain features of the fronts studied in FASINEX. There is a subsurface minimum of potential vorticity on the warm side of the front (Figure 1c).

3.1. Frontogenesis Forced by an External Convergence Field in the Absence of Mixing

In the absence of vertical mixing for a purely two-dimensional situation the semigeostrophic equations apply exactly. To evaluate how Ekman layers influence frontogenesis, we start by considering frontogenesis caused by an external convergence field in the absence of mixing. As by HB, this external convergence field represents the effects of an unstable baroclinic wave on the cross-front structure. HB showed that a singularity in the vorticity occurs in finite time. This happens after 77 hours for a typical oceanic density section with a horizontal convergence field of $\alpha = 1 \times 10^{-5} \text{ s}^{-1}$ representing frontogenesis from mesoscale eddy-like features [*MacVean and Woods*, 1980; *Bleck et al.*, 1988]. The ageostrophic effects

can be understood by considering the along-front momentum balance. As the density gradient increases, the along-front flow accelerates at the surface (through the thermal wind balance). As the along-front flow accelerates, the across-front flow increases at the surface (toward the dense side of the front) and enhances the convergence field. This result also suggests that the singularity should occur first on the dense side of the front.

For purely inviscid flow the front sharpens at the surface as predicted by the simpler analytic solution of HB (Figure 2). With $\alpha = 10^{-5} \text{ s}^{-1}$ in (12) and (13) a discontinuity forms after ~ 2 days. As predicted, the discontinuity forms first on the dense side of the front. For this choice of convergence the vertical velocity grows to more than 38 m d^{-1} after 30 hours. The barotropic convergence field drives an ageostrophic inviscid flow, which is thermally direct; dense water sinks, and light water rises (Figure 2c). The progress of frontogenesis is very much as that described by HB and in the oceanographic application of *MacVean and Woods* [1980]. The density anomaly magnitude is maximum at the surface, as is the potential vorticity anomaly. Note that both of these quantities are conserved, barring numerical diffusion.

Comparison between the density field (Figure 2a) and that pictured by *Samelson and Chapman* [1995, Figure 3] after 10 and 15 days shows good qualitative agreement. Their density sections show the same sharpening of the front at the surface. The times for comparison between our calculations and theirs are meaningless because the fully nonlinear three-dimensional model starts with a very small perturbation that must grow to finite amplitude before the steepening of the front can be realized. While qualitatively the barotropic convergence field seems to mimic the influence of a finite amplitude baroclinic wave on the cross-front structure, it does not exactly represent the baroclinic instability process, particularly since our field has no vertical structure. *Samelson* [1993] found that the normal mode instability of this model is very similar to that of the quasi-geostrophic Eady model, which was the original motivation for the construction of the convergence field by HB. After several days of model time the model run must be stopped because the horizontal resolution becomes inadequate as the singularity predicted by HB is approached. *Bleck et al.* [1988] perform a similar calculation with an isopycnal model using oceanographic parameters and show the strengthening of the jet over time as well as the vigorous upwelling associated with the baroclinically forced front of the order of 5 m d^{-1} .

3.2. Ekman Spindown of a Front

Vertical mixing influences the front in several ways. Simple vertical diffusion of momentum and density acts to weaken the front, but the advective influence of the Ekman layers is even more important. If there is geostrophic vertical shear at the surface and a no-stress surface boundary condition, a surface Ekman layer forms with transport to the left of the geostrophic shear. Surface density and momentum are advected toward the dense side of the front, and the location of the maximum density gradient at the surface is moved toward that side. In addition, there is increasing Ekman transport toward the center of the front approaching it from the light side, which decreases again on the dense side, creating a convergent flow and downwelling below the surface expression of the front. This pattern is controlled by the boundary condition at the surface on the ageostrophic flow, (16) and (17). The vertical geostrophic shear at the surface is proportional to the cross-front density gradient through the thermal wind relationship. Thus,

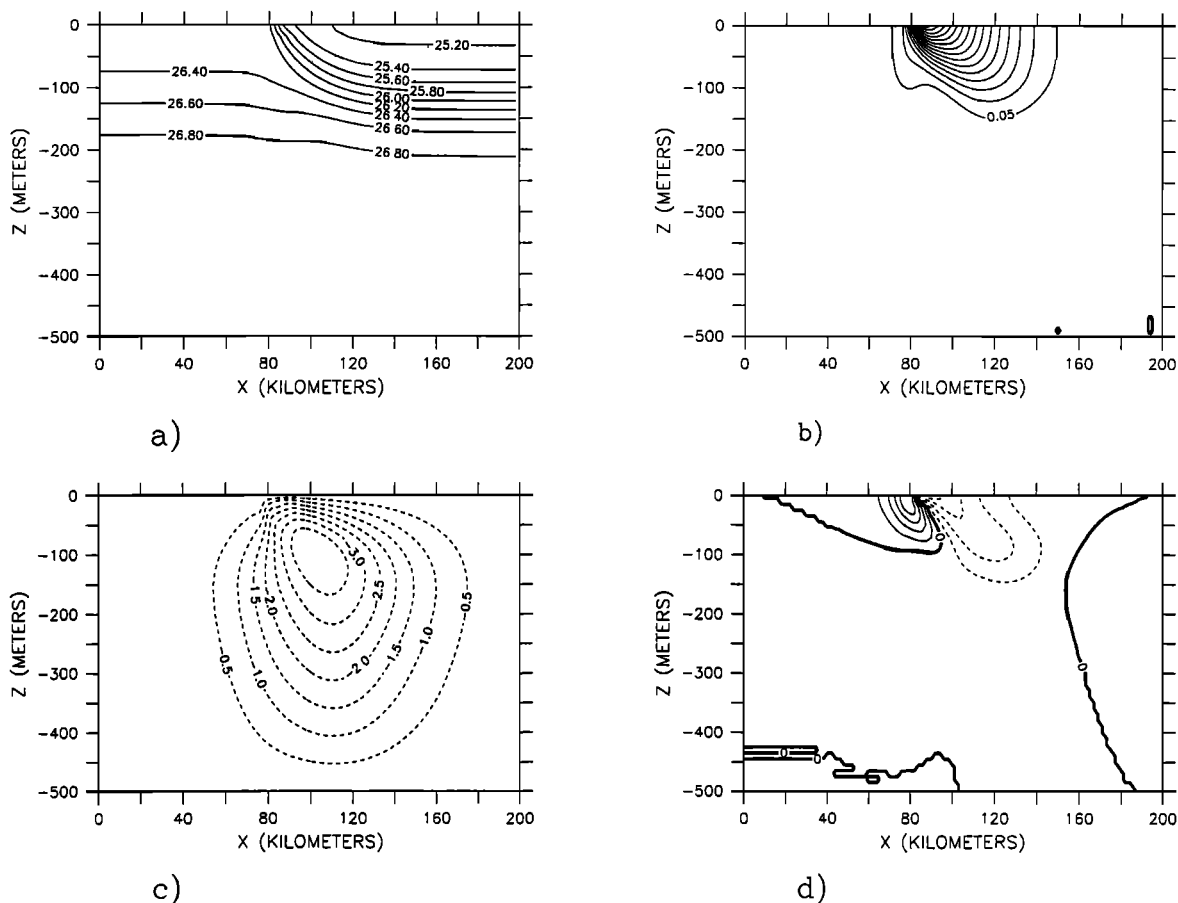


Figure 2. The structure of the solution after 25 hours with no vertical mixing with a barotropic convergence field applied with magnitude $1 \times 10^{-5} \text{ s}^{-1}$: (a) density, (b) geostrophic velocity, (c) ageostrophic cross-front stream function ($\text{m}^2 \text{ s}^{-1}$), and (d) density anomaly from initial conditions.

whenever there is a surface density gradient, one would expect a cross-front ageostrophic flow. The magnitude of this flow depends on the strength of the density gradient. Therefore it will be the strongest at the surface in most ocean fronts. The magnitude of the vertical velocity is given by the convergence of the Ekman flux and thus is proportional to the curvature in the surface density profile. This relationship is given by *Garrett and Loder* [1981, equation (3.8)] and by

$$w = \frac{g\nu}{f^2\rho_0} \frac{\partial^2 \rho}{\partial x^2}. \quad (26)$$

A consequence of the resulting Ekman advection is that the front evolves asymmetrically (Figure 3). The front tips over instead of decaying smoothly in the vertical. The Ekman flux provides an advective influence (Figures 3c and 3d) that causes the strong gradients to remain near the surface. This suggests that the inclusion of vertical mixing of density and momentum is not enough to ensure the formation of a front in equilibrium with forcing and is consistent with the density balance found by *Rudnick* [1996] in observations. The maximum vertical velocity given by this is $\sim 5 \text{ m d}^{-1}$, while the numerical model run gives a maximum vertical velocity of 2.5 m d^{-1} , giving at least an order of magnitude agreement with the scaling.

As time progresses, the light water moves to the left, lightening the surface locally and strengthening the density gradient on the dense side of the front. The surface horizontal density

gradient increases with time (Figure 3a, see also Figure A1) along with the maximum vertical velocity (Figure 3e). As a consequence, there is a large downward bowing of the isopycnals below the largest surface density gradient, and a region of weak stratification (and low potential vorticity) forms, while the potential vorticity at the surface increases because of an increase in stratification (Figures 3h and 3i). The maximum along-front geostrophic velocity does not increase, however, because while the shear at the surface increases, the shear at depth decreases, resulting in a smaller surface velocity at the front. The surface jet splits into two, with the additional jet moving to the left with the surface density front. In the appendix an equation is derived for the evolution of the surface density (ignoring density diffusion relative to advection by the Ekman layers), and a solution is found. The evolution of the surface density profile in the analytic model is qualitatively

Figure 3. (opposite) The structure of the solution after 5 days when there is no external forcing but vertical mixing is applied: (a) density deviation, (b) geostrophic velocity, (c) ageostrophic cross-front stream function, (d) across-front ageostrophic flow in m s^{-1} (contour interval is 0.005 m s^{-1}), (e) vertical velocity times $1 \times 10^5 \text{ m s}^{-1}$, (f) ageostrophic along-front flow (same units as in Figure 3c), (g) density anomaly, (h) potential vorticity, and (i) potential vorticity anomaly.

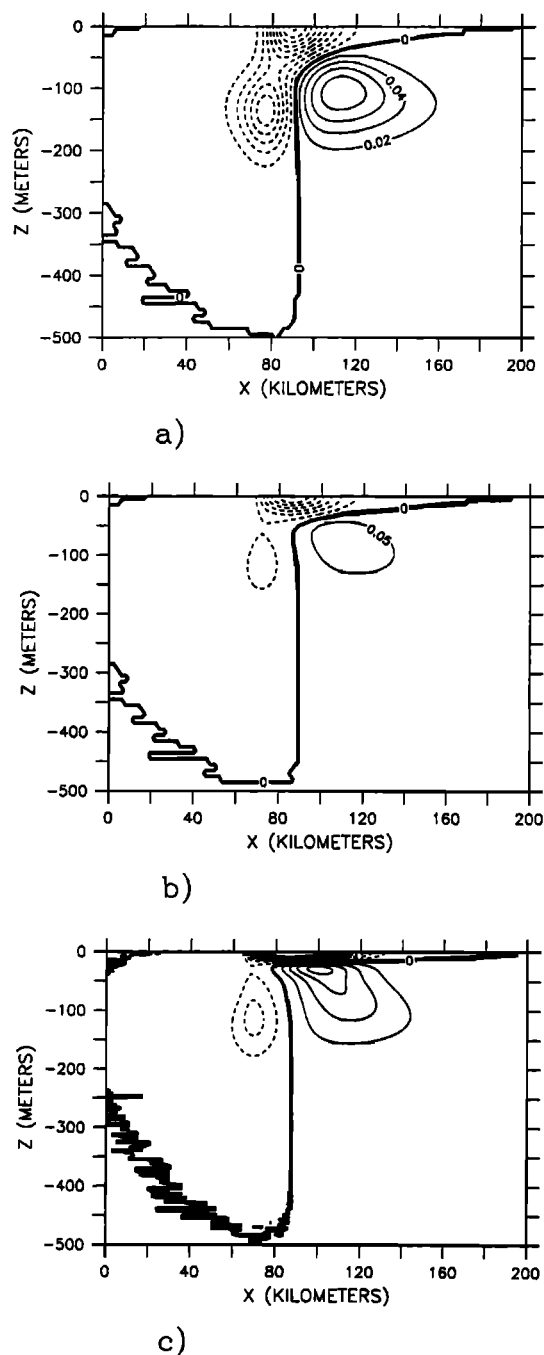


Figure 4. Density anomaly for three different values of friction: (a) $\nu = 0.5 \text{ m}^2 \text{ s}^{-1}$ after 20 hours, (b) $\nu = 0.05 \text{ m}^2 \text{ s}^{-1}$ after 5 days, and (c) $\nu = 0.005 \text{ m}^2 \text{ s}^{-1}$ after 17 days (contour interval is 0.01).

similar to that found in the numerical model, at least in the initial stages. After the near-surface part of the front is sheared away the approximations leading to the analytic solution are violated (in particular, that the depth of the front becomes comparable to the Ekman layer depth), and we expect that at that point the analytic solution is no longer useful.

The inclusion of vertical mixing causes a downward bowing of isopycnals beneath the surface manifestation of the front (Figures 3a and 3g). This feature can be seen in the FASINEX data [Pollard and Regier, 1992] as well as in the Azores front

[Rudnick and Luyten, 1996]. They show nine density sections across the front and define a layer between two isopycnals (25.7 and 25.8 kg m^{-3}). This layer has a local maximum in thickness in six of the nine density sections. We suggest here that this thickness anomaly is caused by frictionally driven convergence. A high in potential vorticity results on the warm side of the front near the surface, creating a subsurface minimum. This is reminiscent of features seen in the Azores front [Rudnick and Luyten, 1996, Plate 2] but not in the FASINEX front [Pollard and Regier, 1992], possibly because of the lack of resolution near the surface. With more vigorous mixing of density in the mixed layer we might expect that the potential vorticity would approach zero there, giving more agreement with the results of Pollard and Regier, [1992]. Although the details of the vertical mixing may be quantitatively important in determining, in particular, the timescale for the growth of this anomaly, the divergence resulting from the vertically integrated Ekman layer transport should be qualitatively independent of the value of the friction coefficient and the form that friction takes. To show this, the value of the frictional parameter was increased by a factor of 10, and while the anomaly in the density field reaches deeper and appears more quickly, the results are qualitatively similar (Figure 4). Likewise, when the parameter is 10 times smaller, the feature is weaker and appears at a later time but once again has qualitative similarities with the runs with larger values of the frictional parameter.

A model run done using the initial conditions of MacVean and Woods [1980] also shows the same density anomaly on the cold side of the front. This density initial condition has a stronger stratification at depth and a larger-scale density gradient (Figure 5).

When vertical mixing and an external barotropic convergence field are applied, downward bowing of isopycnals beneath the surface expression of the front persists. The vertical velocity is stronger with the two effects working together, creating a large thickness anomaly (Figure 6). This suggests that this feature should persist even in the presence of an actively baroclinically unstable field, such as in the ocean. It is difficult to make direct comparisons to the observations since we do not know the appropriate initial conditions and forcing field, but the qualitative similarities suggest that we have captured an important effect.

3.3. Evolution of a Front With Wind Forcing

Ekman flux driven by a wind stress curl can force frontogenesis as well [e.g., Cushman-Roisin, 1981] and is thought to play an important role for large-scale fronts in the ocean. For small-scale fronts it is more interesting to consider how a uniform wind field influences a density front since atmospheric length scales are most often much greater than the length scales associated with density fronts. This case was studied by Adamec and Garwood [1985]. They used a two-dimensional model including horizontal mixing explicitly with a coupled one-dimensional mixed layer model. We revisit the experiments of Adamec and Garwood [1985] with our model, taking into account vertical mixing and allowing vertical shear in the upper ocean, to consider two cases, one in which the wind blows along the front in the direction of the geostrophic jet and the other in which the wind is applied in the opposite direction. In either case, wind-driven Ekman transport is to the right of the wind field, advecting the near-surface density. This flow must compete against the tendency for frictionally induced Ekman layers to move the location of the surface front.

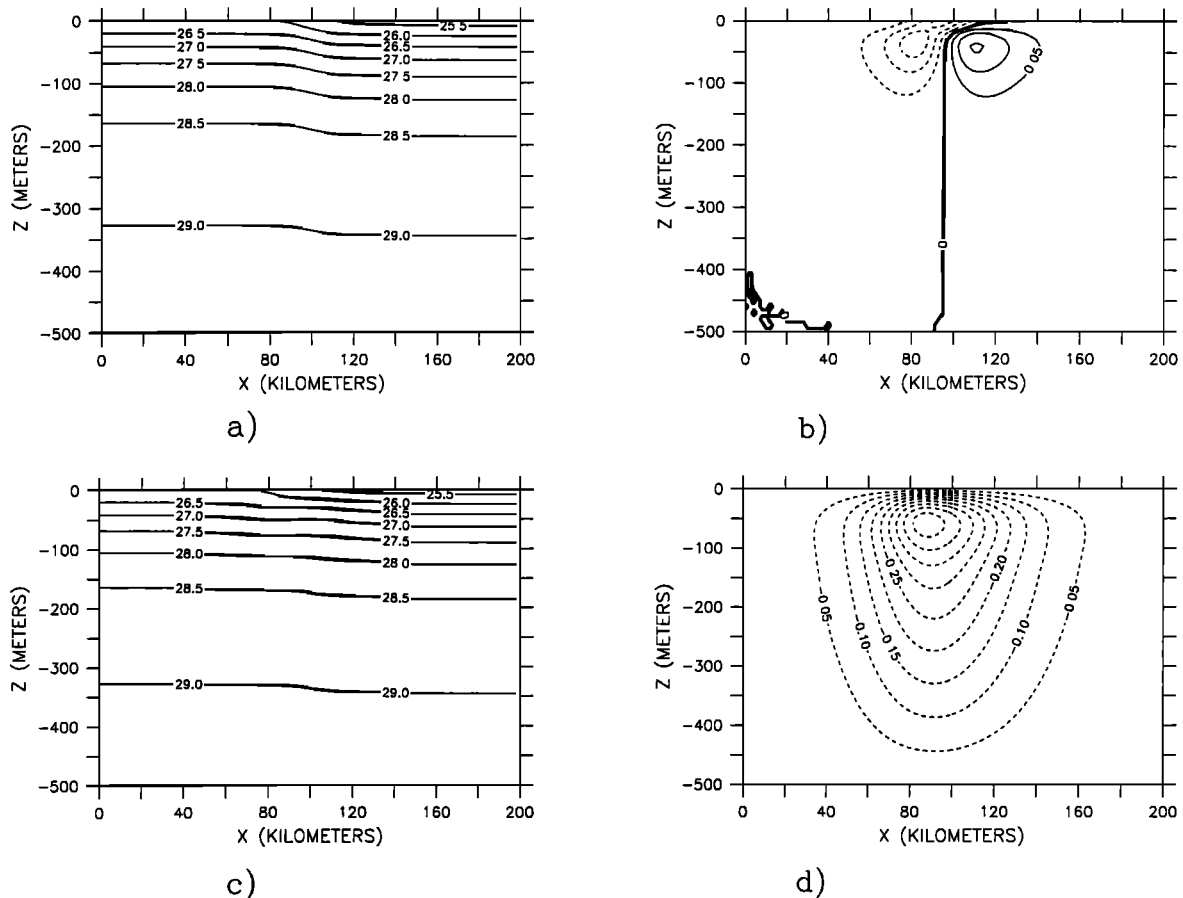


Figure 5. Structure after 150 hours: (a) density initial condition, (b) density anomaly, (c) density, and (d) stream function.

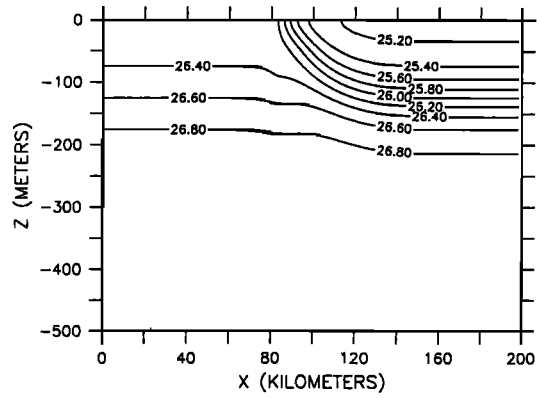
3.3.1. Evolution of a front with uniform wind forcing: Down front wind. When the wind blows along the front (positive) in the direction of the geostrophic current, the Ekman transport to the right of the wind tends to move dense water over lighter water on the right-hand side of the front. However, this flow is in opposition to the frictionally driven flow. This causes a halt to the movement of the density front. The density field becomes slightly statically unstable, and convective adjustment and associated mixing occur (Figure 7). The surface jet diminishes initially over time but later increases as the frictionally driven flow acts to enhance the density gradients and the jet (Figure 8). This situation was simulated by *Adamec and Garwood* [1985], who commented on the movement of the surface jet and also on an associated weakening of the jet in their model. The subsequent strengthening of the jet is not seen in their model. The discrepancy between the two models may be due to the horizontal mixing included in the *Adamec and Garwood* [1985] model and the lack of vertical shear near the surface in their model. There is a slight increase in the potential vorticity gradient near the surface.

3.3.2. Evolution of a front with a uniform wind forcing: Up front wind. When the wind blows in the direction opposite to the surface jet (negative), light water is brought over dense, and the top of the front is sheared away from the deeper portion of the front (Figure 9). Thus the vertical stratification increases locally. We can apply the analytic theory developed in the appendix to understand the influence of the wind. How-

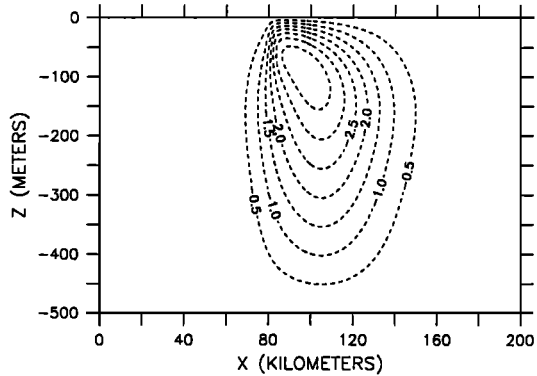
ever, the assumptions behind the analytical model break down quickly because the frontal structure becomes confined to the region of the Ekman layer as the top of the front is shorn off and vertical mixing of density becomes important. In this case the maximum jet velocity decreases uniformly as the density gradient at the surface remains approximately the same (Figure 8), while the geostrophic velocity decreases because of the reduced density gradient at depth. We do not necessarily expect that a discontinuity will form in the surface density gradient as predicted by the analytical model because the model breaks down when the vertical length scale of the front and the Ekman layer become comparable. A model run was done with a domain of 400 km, and the results were nearly identical. The potential vorticity increases substantially near the surface as the density gradient increases because of density advection.

4. Geostrophic Momentum Approximation

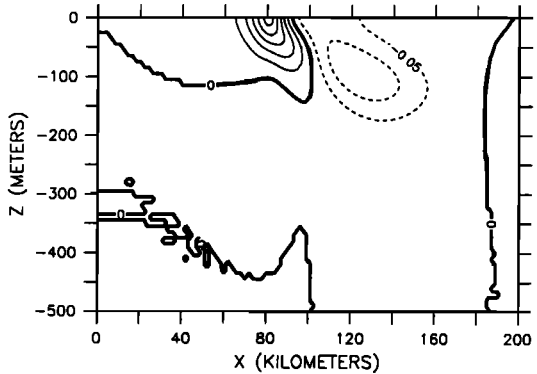
To evaluate whether the approximations leading to the geostrophic momentum approximation are valid for this problem, we reexamine the meridional momentum balance. The Coriolis force on the ageostrophic velocity dominates everywhere. The question remains, however, whether the acceleration of the ageostrophic flow is bigger than the geostrophic acceleration. Everywhere the ageostrophic tendency is an order of magnitude smaller, except near the zero in the geostrophic acceleration. At the point $x = 80$ the two are close in size,



a)



b)



c)

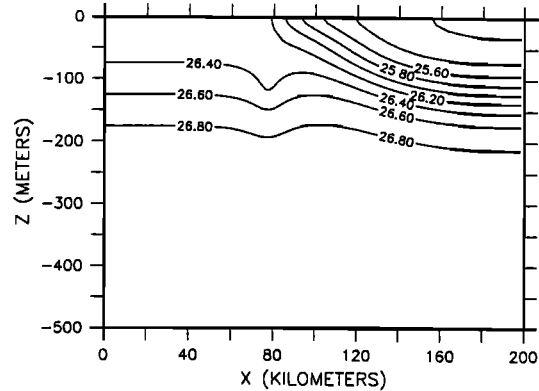
Figure 6. Structure after 25 hours with both external convergence field and vertical mixing: (a) density, (b) stream function, and (c) density anomaly.

but the geostrophic acceleration still dominates (Figure 10). This suggests that the approximation for the most part is valid. It is interesting to note that the primary balance in the zonal momentum equation is the same as that suggested by *Lee et al.* [1994, equation (21)] for their nonhydrostatic model, which is a balance between cross-front flow and vertical mixing of momentum. This suggests that the approximations used in this paper may be appropriate for looking at the dynamics of fronts and provides a useful dynamical formalism that lies in between quasi-geostrophic (which has been used extensively for the analysis of observations) and full nonhydrostatic dynamics. In

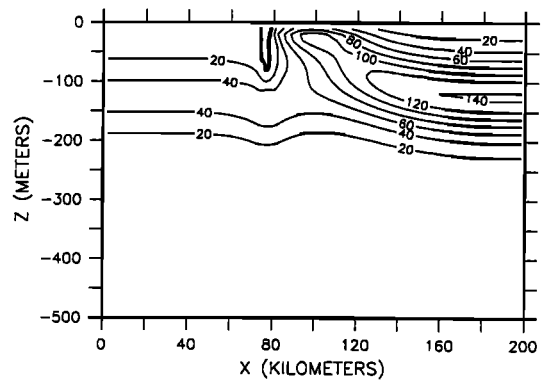
addition, the qualitative agreement in the density equation with the results of *Rudnick* [1996] also suggests that the dynamics used in this study have some validity.

5. Conclusions

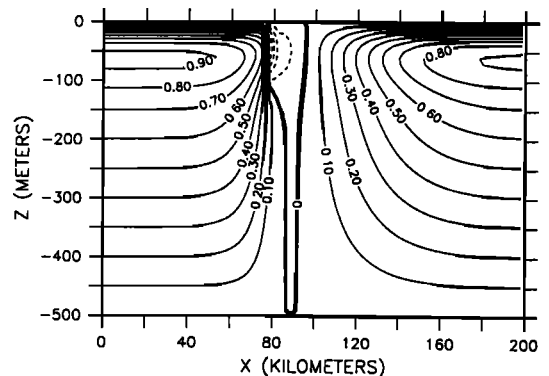
We have modified the semigeostrophic model to include vertical mixing of density and momentum in a simple way and used the model to study frontogenesis and frontolysis. The vertical mixing influences the evolution of the front in ways more complex than simple diffusion of density and momen-



a)



b)



c)

Figure 7. Structure after 7.5 days with wind in the direction of the surface jet and with wind stress having a value of 0.1 Pa: (a) density, (b) potential vorticity, and (c) stream function.

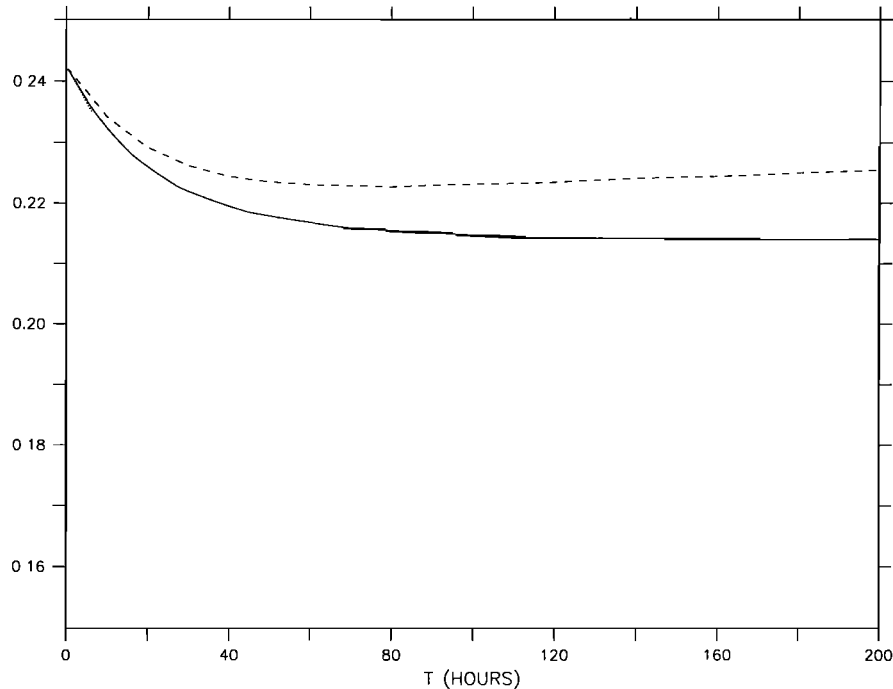


Figure 8. Maximum geostrophic velocity for positive wind stress (dashed line), no wind stress (solid line), negative wind stress (dotted line).

tum. In the absence of vertical mixing, for the application of a barotropic convergence field such as would arise from baroclinic instability of the thermocline (as expected from the results of HB), the vorticity is greater on the dense side of the front than on the light side of the front. In the absence of external forcing, either by the wind or by a barotropic convergence field, the viscosity acts to spin down a front but in a nonuniform way. Because a no-stress boundary condition is applied at the surface, there is a convergent Ekman flux that forms in response to the geostrophic shear at the surface. This shear is balanced by shear from the ageostrophic velocities in the Ekman layer. The resulting net overturning circulation tends to tilt over the front. The maximum density gradient moves in the negative x direction (toward the dense side of the front), and the surface horizontal density gradient remains large even after the front has shifted by a significant amount. In the appendix we show that a discontinuity in density gradient can form when the vertical scale of the stratification is greater than the Ekman layer thickness; this is a similar approximation to that studied by *Garrett and Loder* [1981] whereby vertical mixing of density is neglected but advection by Ekman layers is retained. This scaling seems consistent with the observational results of *Rudnick* [1996]. The solution shows that a two-dimensional front does not equilibrate in the presence of vertical mixing alone, and under this approximation, discontinuities form at the surface after a finite period of time. Thus it seems that vertical mixing alone may not be able to equilibrate a two-dimensional front; horizontal mixing is needed as well. However, the approximation leading to the analytical solution breaks down after the part of the front in the Ekman layer is sheared off from the subsurface expression of the front and the thickness of the Ekman layer becomes comparable to the thickness of front. At this point, vertical diffusion must become important, and a surface discontinuity does not form.

There are several potential deficiencies in our modeling approach. The model that we use to study this process is purely two-dimensional. Clearly, in the ocean, baroclinic instability breaks the along-front symmetry. Thus the quantitative results of the model are suspect after several e -folding times for the baroclinic instability of the frontal feature. However, for the elevated value of vertical mixing used here, there could be order one changes in the front before a finite amplitude wave would develop. In addition, after the along-front structure begins to evolve the effects of vertical mixing would still persist. The finite size of the model domain could also influence the solution, although the open boundary conditions appear from visual inspection to be working well and several experiments were done with larger model domains that gave approximately the same solution. Because the semigeostrophic approximation eliminates gravity waves from the dynamics, there are no problems with waves reflecting off of the boundaries, which makes the open boundary conditions robust. Of course, the simplicity of the mixing parameterization is questionable. However, it does allow an examination of the influence of vertical mixing along with vertical shear in the upper ocean that other models have missed. The size of the frictional coefficient should not effect the qualitative conclusions of the study, although quantitatively, since the vertical velocity in (26) is proportional to ν , the timescale of evolution of the front should depend linearly in the friction coefficient. Tests with two other values of frictional coefficient confirm this conjecture. Tests of the zonal momentum balance confirm that in this situation the semigeostrophic equation is appropriate.

Several predictions from the model seem to be born out by observations. First, because of the convergent Ekman flux, there is a downward bowing of isotherms beneath the region of maximum horizontal density gradient at the surface. This feature appears in observations of the FASINEX and the Azores

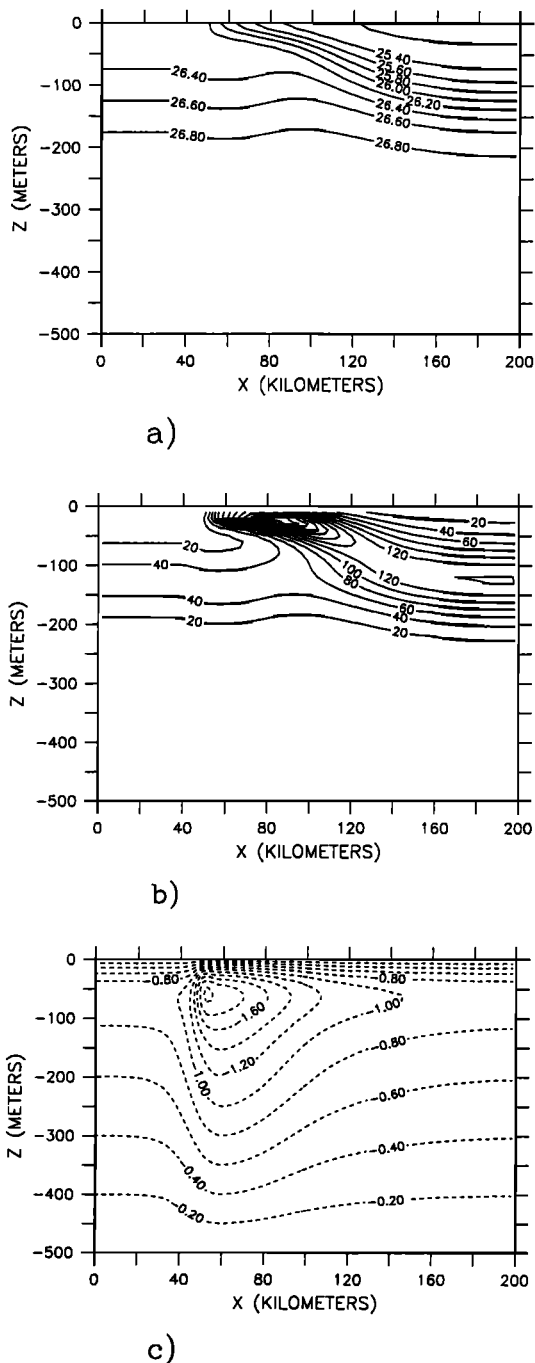


Figure 9. Same as Figure 7 but with negative wind stress.

fronts. However, there are other ways in which this downward bowing of isopycnals could appear in a horizontal section of density at a front. For instance, simulations of the nonlinear evolution of a baroclinically unstable front show similar structures, with downward bowing of isopycnals at depth. This feature appears in a density section as the front meanders, and part of that meander is captured by the section. However, the density and potential vorticity anomaly (associated with the displaced isopycnals) tends to be located away from the surface expression of the front [see e.g., *Samelson and Chapman*, 1995, Figure 3]. A comparison between the potential vorticity signal of *Samelson and Chapman* [1995, Figure 21a] and that derived

by *Pollard and Regier* [1992, Figure 16] further shows these differences, with a low in potential vorticity appearing below the surface expression of the front of *Pollard and Regier's* [1992] calculation and a high appearing in the front of *Samelson and Chapman's* [1995] calculation. We find here that the density anomaly (and resulting potential vorticity anomaly) occurs directly below the surface expression of the front (as found in the observations). The comparison, of course, is only valid in regions of convergence in the baroclinically unstable waves. In addition, the region of high potential vorticity on the cold side of the front also appeared in the sections of the Azores front shown by *Rudnick and Luyter* [1996]. It is therefore important to consider the strength of the frictionally driven flow. With the canonical value of mixing coefficient the vertical velocity associated with frictionally driven Ekman layers is of the order of 5 m d^{-1} , while baroclinic instability and convergence estimates give $\sim 30 \text{ m d}^{-1}$ [*Pollard and Regier*, 1992; *Samelson and Chapman*, 1995]. This suggests that the frictional effects are small. The frictionally driven convergence scales (approximately) with the friction coefficient. However, the comparisons to the observations are compelling and suggest that they could be important, particularly near the front.

In order to understand the dynamics of the front, *Pollard and Regier* [1992] derive the vertical overturning circulation by solving the Omega equation [*Pollard and Regier*, 1992, equation (5.10)]. The assumptions leading to this equation are that the along-front flow is geostrophic and has no along-front variations and that the flow is inviscid. From the geostrophic velocities derived from the density they derive a confluence field to find the appropriate forcing term (equivalent to (13)). The resulting overturning stream function bears some resemblance to that found here (e.g., Figures 2c and 3c); however, there is one possible difference. In *Pollard and Regier's* [1992] Figure 16 the overturning stream function is plotted over the potential vorticity, and there is a suggestion that the upward vertical velocity starts in the region of low potential vorticity and downward bowing of the isopycnals. This could have occurred because of inherent errors in their calculations but does suggest that the inclusion of frictional convergence could possibly make the cross-front circulation picture more consistent with the density and potential vorticity field.

The differences between the response of the front to down front versus up front wind are suggested by the work of *Lee et al.* [1994]. Because we have filtered out gravity waves and inertial oscillations, we found that in the down front wind case the frontal region can be arrested by the competition between frictionally driven convergence and the movement of the front by the surface wind-driven Ekman flux. In the up front wind case a region of high potential vorticity is formed once again on the cold side of the front, with a structure that looks fairly similar to that with strong vertical mixing alone, as suggested by the analytical model in the appendix.

Although the cross-frontal circulation represents fluid parcels paths, the concentration of a tracer (such as density) would be continually diffused in the vertical and thus may lose the signature of its surface properties rather quickly. It appears, however, that when vertical mixing is high, Ekman layer advection dominates over vertical diffusion. Thus, having large vertical mixing in the upper ocean does not necessarily mean that there should be a rapid weakening in horizontal density gradients. Also, it seems reasonable to model mixing as vertical in the upper ocean, but at some depth, the mixing should be

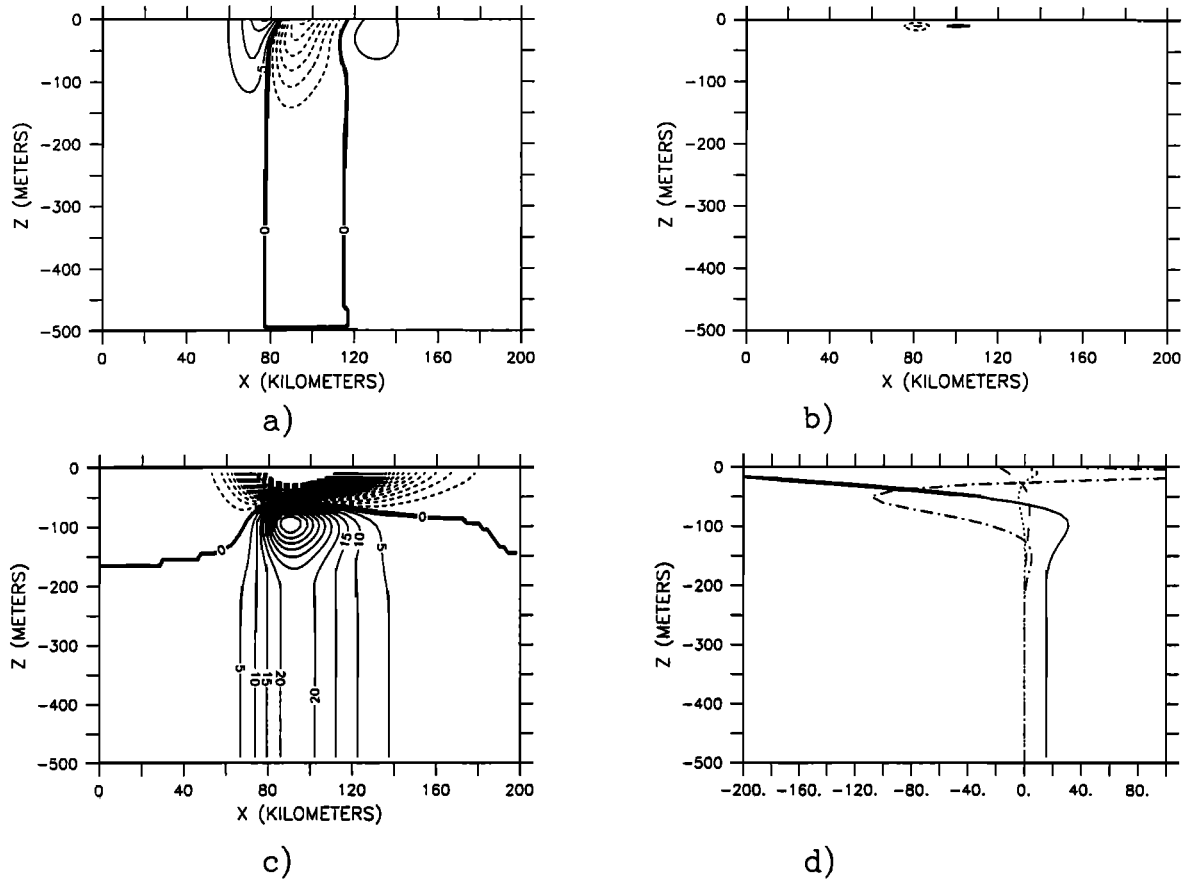


Figure 10. Terms in the along-front momentum balance times 1×10^8 in units of s^{-1} with a contour interval of 5: (a) geostrophic velocity tendency, (b) ageostrophic (along-front) velocity tendency, (c) Coriolis force on the cross-front flow, and (d) each of the terms at $x = 80$ km (where the ageostrophic velocity tendency is maximum), Coriolis force on the cross-front flow (solid line), geostrophic velocity tendency (dashed line), ageostrophic velocity tendency (dotted line), and Coriolis force on the along-front ageostrophic flow (dash-dotted line).

modeled as diapycnal instead. How that transition occurs is unclear.

In order to draw more conclusions about how fronts work in the real ocean, one would want to include realistic mixed layer dynamics; however, it appears that vertical shear in the upper ocean near fronts may play an important role in the dynamics. This is not allowed in traditional slab mixed layer models where both the velocity and density are assumed to be uniform in the vertical within the mixed layer. Allowing a vertical shear within the mixed layer is consistent with the approaches of *Tandon and Garrett* [1994] and *Young* [1994] and is supported by observations. Although the parameterization for mixing that we assume here is quite simple, it does introduce an important effect and provides a dynamical framework for some observed features of oceanic fronts.

Appendix A

In this appendix an analytical solution is derived for the evolution of a density front at the surface in the presence of vertical mixing of density and momentum. Consider the density equation (16). At the surface, (16) reduces to

$$\frac{\partial \rho}{\partial t} + u \frac{\partial \rho}{\partial x} = \kappa \frac{\partial^2 \rho}{\partial z^2} \quad (\text{A1})$$

because of the no-heat flux condition at the surface. To simplify (A1) further, consider the relative sizes of the second and third terms. To scale the horizontal velocity u , notice that near the surface, within the Ekman layer, we can assume that the cross-front flow is given by the Ekman layer dynamics. If the Ekman layer is driven by a surface stress, then the Ekman solution gives the velocity at the surface as

$$u = \frac{1}{\sqrt{f\kappa}} \frac{\tau^y}{\rho_0} \frac{\sqrt{2}}{2}. \quad (\text{A2})$$

In the absence of wind stress the surface boundary condition requires that the total stress goes to zero. In that case the surface boundary condition is given by (17):

$$u = -\frac{\nu}{\sqrt{f\kappa}} \frac{\sqrt{2}}{2} \frac{\partial v_\theta}{\partial z}. \quad (\text{A3})$$

The geostrophic shear at the surface is in turn related directly to the cross-front density gradient. The relative size of the vertical diffusion of density to the horizontal advection can now be estimated as

$$\frac{|\kappa \rho_{zz}|}{|u \rho_x|} = \frac{L^2 f^2 \rho}{g \Delta \rho H^2} \sqrt{\frac{2\kappa}{f}}, \quad (\text{A4})$$

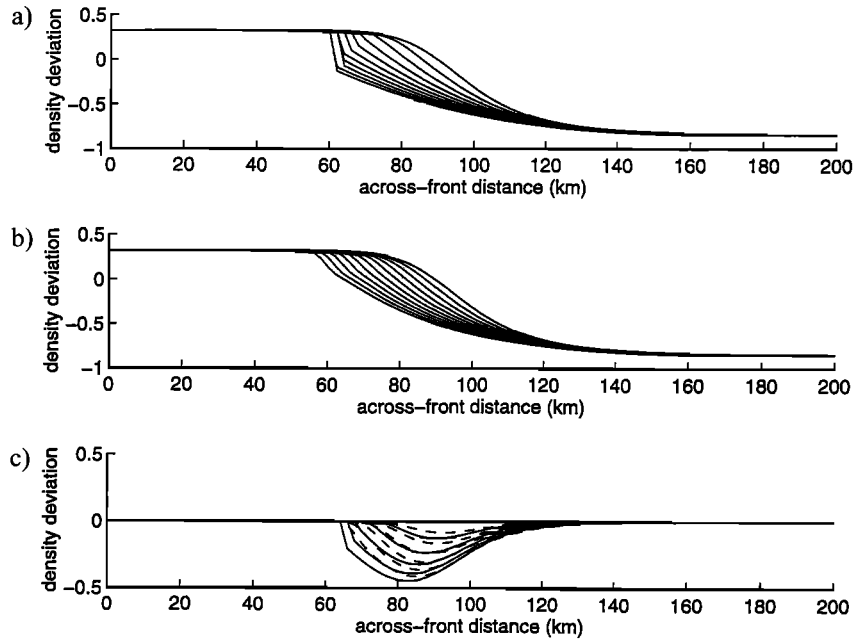


Figure A1. Density distribution every 24 hours with no external forcing applied for 10 days: (a) distribution predicted from the analytical model, (b) distribution from the numerical model, and (c) distribution of density subtracted from the initial density profile every 24 hours for the analytical model (solid lines) and numerical model (dashed lines).

where L is the horizontal length scale of the variation in surface density, H is the depth scale of the density change of the front, $\Delta\rho$ is the horizontal density change of the front (which is assumed to be the same as the density change in the vertical), and the Prandtl number is 1. This expression is equivalent to

$$\frac{|\kappa\rho_{zz}|}{|u\rho_x|} = B \frac{\delta_e}{H},$$

where $B = (L^2 f^2) / (N^2 H^2)$ is the Burger number times the Ekman layer depth divided by the vertical scale of the density stratification. If this number is small, that is, if the Burger number is of order one or less, and the Ekman layer depth is much less than the vertical scale of density changes, then the equation governing the surface density distribution becomes

$$\frac{\partial\rho}{\partial t} + u\rho_x = 0 \tag{A5}$$

or

$$\frac{\partial\rho}{\partial t} + \frac{g\kappa}{\rho_0 f} \frac{1}{\sqrt{2f\kappa}} \rho_x^2 = 0. \tag{A6}$$

This is a first order nonlinear partial differential equation that can be solved by the method of characteristics. If we scale the solution such that

$$T^{-1} = \frac{B\delta_e}{2H} f$$

or, equivalently, by

$$T^{-1} = \frac{g\Delta\rho\delta_e}{2\rho f L^2},$$

then we have

$$\frac{\partial\rho}{\partial t} + \rho_x^2 = 0. \tag{A7}$$

If the initial condition for (A6) is $\rho = G(x)$, then the solution to (A6) can be written as an implicit set of equations given by

$$x = 2G'(s)t + s \tag{A8}$$

$$\rho = G(s) + [G'(s)]^2 t, \tag{A9}$$

where the prime indicates a derivative with respect to the argument and s is a dummy variable. To solve this set of equations, we solve for s as a function of x and t from (A8) and, so, find ρ as a function of x and t .

As a simple example, consider the case where there is initially a uniform gradient $\rho = \beta x$. We find that in that case, $s = x - 2\beta t$ and $\rho = \beta x - \beta^2 t$, so there is still a linear gradient in x and no discontinuity forms.

If we consider a more general density profile at the surface, one where the density gradient is confined locally (for instance, $\rho = \tanh(x)$), then we are able to find a solution to the above system of equations as long as

$$1 + 2G''(s)t = 0. \tag{A10}$$

This is a requirement of the Jacobian of the transformation used to find the solution. The second derivative of the initial density profile must go through zero if the gradient has no discontinuities in it (at least through the second derivative) and the density approaches a constant away from the front. For some time t , (A10) must hold. At that point the solution is no longer unique, and a discontinuity must form. This suggests that if (A7) holds, then a frontal discontinuity should form from the influence of the Ekman advection (in the absence of wind). Since the discontinuity is in the horizontal, vertical mixing of density may not remove it. As an example, for $\rho = \tanh(x)$ a discontinuity forms when

$$1 + 4 \operatorname{sech}^2 s \tanh st = 0. \tag{A11}$$

This happens first for $t = 0.6495$ and $x = -0.65835$. We can also apply (A11) to the surface density profile defined in (24). The evolution of the surface density as a function of time from the numerical model run pictured in Figure 3 gives a rather smooth evolution. The surface density evolution predicted from (A8)–(A9) shows a discontinuity in the surface horizontal density gradient that continues to grow (Figure A1a). The timescale for this distribution is 7000 hours. The discontinuity is predicted to form after 53 hours. The numerical solution shows a similar behavior, with a more gentle discontinuity forming (Figure A1b). The numerical solution also evolves more slowly (Figure A1c) but has the same character as the analytic solution.

The solution can also include a uniform wind stress that is in the direction opposite to the surface jet. In that case the analytical solution still shows a discontinuity forming; however, it occurs farther to the dense side of the front because (A10) is modified to

$$x = st + 2G'(s)t + \tau. \quad (\text{A12})$$

Equation (A12) also suggests the arrest of the front when the wind is down the jet.

Acknowledgments. This work began while the author was a College of Oceanography and Fisheries Sciences postdoctoral fellow at the University of Washington and was completed under an Office of Naval Research Young Investigator Program Award. She acknowledges useful conversations with Daniel Rudnick, Fiamma Straneo. Comments by Amit Tandon and an anonymous reviewer are also gratefully acknowledged.

References

- Adamec, D., and R. W. Garwood, The simulated response of an upper ocean front to local atmospheric forcing, *J. Geophys. Res.*, **90**, 917–928, 1985.
- Bleck, R., R. Onken, and J. D. Woods, A two-dimensional model of mesoscale frontogenesis in the ocean, *J. R. Meteorol. Soc.*, **114**, 347–371, 1988.
- Boss, E., N. Paldor, and L. Thompson, Stability of a potential vorticity front: From quasi-geostrophy to shallow-water, *J. Fluid Mech.*, **315**, 65–84, 1996.
- Cushman-Roisin, B., Effects of horizontal advection on upper ocean mixing: A case of frontogenesis, *J. Phys. Oceanogr.*, **11**, 1345–1356, 1981.
- Eriksen, C. C., R. A. Weller, D. L. Rudnick, R. T. Pollard, and L. A. Regier, Ocean frontal variability in the Frontal Air-Sea Interaction Experiment, *J. Geophys. Res.*, **96**, 8569–8592, 1991.
- Garrett, C. J. R., and J. W. Loder, Dynamical aspects of shallow sea fronts, *Philos. Trans. R. Soc., London, Ser. A*, **302**, 563–581, 1981.
- Hoskins, B. J., The geostrophic momentum approximation and the semigeostrophic equations, *J. Atmos. Sci.*, **32**, 233–242, 1975.
- Hoskins, B. J., and F. P. Bretherton, Atmospheric frontogenesis models: Mathematical formulation and solution, *J. Atmos. Sci.*, **29**, 11–37, 1972.
- Lee, C. M., and C. C. Eriksen, The subinertial momentum balance of the North Atlantic Subtropical Convergence Zone, *J. Phys. Oceanogr.*, **26**, 1690–1704, 1996.
- Lee, D. K., P. Niiler, A. Warn-Varnas, and S. Piasek, Wind-driven secondary circulation in ocean mesoscale, *J. Mar. Res.*, **52**, 371–396, 1994.
- MacVean, M. K., and J. D. Woods, Redistribution of scalars during upper ocean frontogenesis: A numerical model, *Q. J. R. Meteorol. Soc.*, **106**, 293–311, 1980.
- Pollard, R. T., and L. A. Regier, Vorticity and vertical circulation at a front, *J. Phys. Oceanogr.*, **22**, 609–625, 1992.
- Roden, G. I., On the subtropical frontal zone east of Hawaii during winter, *J. Phys. Oceanogr.*, **10**, 342–362, 1980.
- Rudnick, D., Intensive surveys of the Azores front, 2, Inferring the geostrophic and vertical velocity fields, *J. Geophys. Res.*, **101**, 16,291–16,303, 1996.
- Rudnick, D. L., and R. E. Davis, Frontogenesis in mixed layers, *J. Phys. Oceanogr.*, **18**, 434–457, 1988.
- Rudnick, D. L., and J. R. Luyten, Intensive surveys of the Azores Front, 1, Tracers and dynamics, *J. Geophys. Res.*, **101**, 923–939, 1996.
- Samelson, R. M., Linear instability of a mixed-layer front, *J. Geophys. Res.*, **98**, 10,195–10,204, 1993.
- Samelson, R. M., and D. C. Chapman, Evolution of the instability of a mixed-layer front, *J. Geophys. Res.*, **100**, 6743–6759, 1995.
- Spall, M. A., Frontogenesis, subduction, and cross-front exchange at upper ocean fronts, *J. Geophys. Res.*, **100**, 2543–2557, 1995.
- Spall, M. A., Baroclinic jets in confluent flow, *J. Phys. Oceanogr.*, **27**, 1054–1071, 1997.
- Tandon, A., and C. Garrett, Mixed layer restratification due to a horizontal density gradient, *J. Phys. Oceanogr.*, **24**, 1419–1424, 1994.
- Voorhis, A. D., E. H. Schroeder, and A. Leetmaa, The influence of deep mesoscale eddies on sea surface temperature in the North Atlantic subtropical convergence, *J. Phys. Oceanogr.*, **6**, 953–961, 1976.
- Young, W. R., The subinertial mixed layer approximation, *J. Phys. Oceanogr.*, **24**, 1812–1826, 1994.

L. Thompson, School of Oceanography, Box 357940, University of Washington, Seattle, WA 98195-7940. (luanne@ocean.washington.edu)

(Received September 3, 1997; revised December 20, 1999; accepted December 20, 1999.)